DISCOVER WHAT'S NEW.

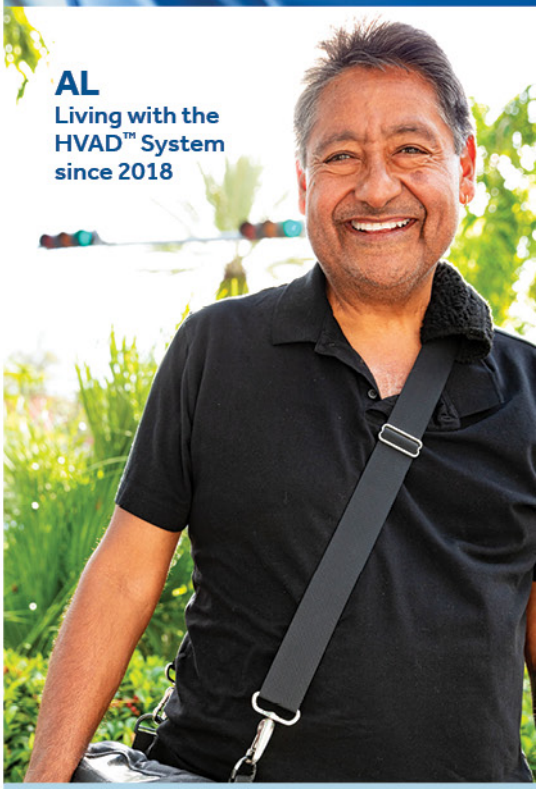

Discover Autologs™ made easier. This is HVAD, enhanced with Autologs 1.3.

Introducing Autologs 1.3, the latest update to our advanced device management service that includes:

- The option to download logfile reports directly from the website, providing faster access to important data.
- A detailed list of alarm and event notifications.
- Convenient summary statistics for easier interpretation of pump performance.

Speak to your Medtronic representative or visit Medtronic.com/DiscoverHVAD to learn more.

Medtronic

Brief Statement
HeartWare™ HVAD™ System
Indications For Use: The HeartWare™ HVAD™ System is indicated for hemodynamic support in patients with advanced, refractory left ventricular heart failure; either as a Bridge to Cardiac Transplantation (BTT), myocardial recovery, or as Destination Therapy (DT) in patients for whom subsequent transplantation is not planned.
Contraindications: The HeartWare System is contraindicated in patients who cannot tolerate anticoagulation therapy.
Warnings/Precautions: Proper usage and maintenance of the HVAD™ System is critical for the functioning of the device. Serious and life-threatening adverse events, including stroke, have been associated with use of this device. Blood pressure management may reduce the risk of stroke. Never disconnect from two power sources at the same time (batteries or power adapters) since this will stop the pump, which could lead to serious injury or death. At least one power source must be connected at all times. Always keep a spare controller and fully charged spare batteries available at all times in case of an emergency. Do not disconnect the driveline from the controller or the pump will stop. Avoid devices and conditions that may induce strong static discharges as this may cause the VAD to perform improperly or stop. Magnetic resonance imaging (MRI) could cause harm to the patient or could cause the pump to stop. The HVAD™ Pump may cause interference with automatic implantable cardioverter-defibrillators (AICDs), which may lead to inappropriate shocks, arrhythmia, and death. Chest compressions may pose a risk due to pump location and position of the outflow graft on the aorta — use clinical judgment. If chest compressions have been administered, confirm function and positioning of HVAD Pump post-CPR.
Potential Complications: Implantation of a VAD is an invasive procedure requiring general anesthesia and entry into the thoracic cavity. There are numerous known risks associated with this surgical procedure and the therapy including, but not limited to, death, stroke, neurological dysfunction, device malfunction, peripheral and device-related thromboembolic events, bleeding, right ventricular failure, infection, hemolysis, and sepsis. Refer to the "Instructions for Use" for detailed information regarding the implant procedure, indications, contraindications, warnings, precautions, and potential adverse events prior to using this device.
Caution: Federal law (USA) restricts these devices to sale by or on the order of a physician.

Received: 2 July 2019 | Revised: 5 October 2019 | Accepted: 7 October 2019

DOI: 10.1111/aor.13593

MAIN TEXT ARTICLE

Artificial Organs WILEY

Computational investigation of hemodynamics in hardshell venous reservoirs: A comparative study

Ali Cemal Benim[1] | **Thiemo Frank**[2] | **Alexander Assmann**[2] | **Artur Lichtenberg**[2] | **Payam Akhyari**[2]

[1]Department of Mechanical and Process Engineering, Duesseldorf University of Applied Sciences—Center of Flow Simulation (CFS), Duesseldorf, Germany
[2]Department of Cardiovascular Surgery, Heinrich Heine University, Duesseldorf, Germany

Correspondence
Ali Cemal Benim, Department of Mechanical and Process Engineering, Duesseldorf University of Applied Sciences—Center of Flow Simulation (CFS), Muensterstr. 156 D-40476, Duesseldorf, Germany.
Email: alicemal@prof-benim.com

Funding information
CORMED Medizintechnik, Rüthen, Germany

Abstract

Extracorporeal circulation using heart-lung-machines is associated with a profound activation of corpuscular and plasmatic components of circulating blood, which can also lead to deleterious events such as systemic inflammatory response and hemolysis. Individual components used to install the extracorporeal circulation have an impact on the level of activation, most predominantly membrane oxygenators and hardshell venous reservoirs as used in extracorporeal systems. The blood flows in two different hardshell reservoirs are computationally investigated. A special emphasis is placed on the prediction of an onset of transition and turbulence generation. Reynolds-averaged numerical simulations (RANS) based on a transitional turbulence model, as well as large eddy simulations (LES) are applied to achieve an accurate prediction. In the LES analysis, the non-Newtonian behavior of the blood is considered via the Carreau model. Blood damage potential is quantified applying the Modified Index of Hemolysis (MIH) based on the predicted flow fields. The results indicate that the flows in both reservoirs remain predominantly laminar. For one of the reservoirs, considerable turbulence generation is observed near the exit site, caused by the specific design for the connection with the drainage tube. This difference causes the MIH of this reservoir to be nearly twice as large as compared to the alternative design. However, a substantial improvement of these performance criteria can be expected by a local geometry modification.

KEYWORDS

computational fluid dynamics, hardshell venous reservoirs, hemolysis

1 | INTRODUCTION

The introduction of extracorporeal circulation using heart lung machine has opened the door to a broad range of cardiac operations that represent the standard repertoire of modern cardiac surgery. However, a standard setup of heart lung machines contains a number of components with increased risk of triggering adverse events, that is, thrombogenesis and hemolysis.[1,2] Here, particularly the oxygenator and the hardshell venous reservoir have been demonstrated to play a major role in blood component activation and respective damage.[3,4] Computational fluid dynamics (CFD) based procedures are being increasingly used to investigate blood flow characteristics. Various computational models, for the vascular blood flow with different emphases, were presented by a number of researchers.[5–11] Computational investigation of the blood flow in artificial organs and biomedical

devices such as heart pumps in various designs has equally attracted attention.[12–15] A further field where CFD approaches have been extensively utilized comprises design engineering and performance monitoring of heart valves.[16–19]

One of the early CFD analyses of oxygenators (including the membrane and the hardshell reservoir) is due to Gage et al,[20] who investigated a commercial membrane oxygenator computationally and experimentally, with emphasis on the pressure drop. A Newtonian behavior for the blood was assumed, along with the assumption of a laminar flow. A further computational investigation of a membrane oxygenator along with X-ray imaging was presented by Jones et al,[21] who again assumed a laminar flow and a Newtonian blood behavior. They placed an emphasis upon the mathematical modelling of the flow through the membrane, modelling the latter as a porous medium. A more detailed modelling of the membrane by resolving the microstructures was performed by Pelosi et al[22] for a prototype hollow-fiber membrane oxygenator with integrated heat exchanger. Here, a Newtonian behavior for the blood was assumed. However, unlike the previously cited analyses[20,21] Pelosi and coworkers[22] assumed blood flow not to be laminar, but considered the presence of turbulence by means of a Reynolds-averaged numerical simulation (RANS) based[23] two-equation model, namely the k-ω model.[24] The emphasis in the latter work was placed on the prediction of the thrombogenic potential resulting from flow-related mechanical factors.[22]

The modelling applied in the present work differs from the previous studies[20–22] in several points. The membrane is not included in the present solution domain. However, the applied models for the fluid flow are more sophisticated. The non-Newtonian blood behavior is considered, and flow turbulence is treated by more accurate models.

In the present study, the flow in two different hardshell venous reservoirs of a cardiopulmonary bypass (CPB) circuit is analyzed, without attempting to model the flow through the closely attached oxygenator membrane. Both reservoirs are commercially available products. Sorin (today: LivaNova, London, UK) Dual Avant has been used in our unit for quite a long time, and LivaNova Inspire has been introduced as a modern alternative. As already pointed out above, hardshell venous reservoirs are known to be a critical component of extracorporeal circulation. Hence, we designed this study with the aim of gaining an increased insight into the changes of predicted hemocompatibility that result from a change in design.

2 | OUTLINE OF THE MATHEMATICAL AND COMPUTATIONAL MODELLING

In the present study, the computational analysis was performed based on the finite volume method (FVM)[25] utilizing the general-purpose CFD code ANSYS Fluent 18.0.[26] Since the oxygenator membrane was not modelled, the solution domain in the present study is the reservoir between the outer surface of the membrane (ie, where the blood leaves the membrane) as the inlet, and the drainage tube as the outlet boundaries. The problem was investigated for a constant flow rate and a constant filling level. Thus, the boundary conditions were in steady-state. The applied boundary conditions will be discussed in the following section, in more detail.

The flow in the hardshell reservoir can exhibit, in general, laminar and turbulent behavior at the same time in different regions, depending on the geometry and operating conditions. Both Gage and Jones and colleagues[20,21] assumed a laminar flow throughout, whereas turbulent flow was assumed in the study of Pelosi[22] based on RANS. In all cases, a Newtonian behavior was assumed for the blood.[20–22] However, as the strain rate can vary over a wide range in the reservoir, exhibiting large differences in flow velocities, the non-Newtonian behavior may not be negligible.

In the present work, an unsteady approach was applied within the framework of an LES formulation, in order to be able to resolve possible transitional/turbulent flow accurately. Here, the so-called implicit LES (ILES) approach was preferred,[27,28] where no subgrid-scale viscosity was used, assuming the numerical dissipation to sufficiently mimic the effect of the unresolved turbulent motion. The non-Newtonian behavior of the blood was considered via the Carreau viscosity model,[29] which assumes the following relationship for the molecular viscosity (μ):

$$\mu = \mu_\infty + \left(\mu_0 - \mu_\infty\right)\left[1+\lambda^2\dot{\gamma}^2\right]^{\frac{n-1}{2}} \qquad [Pa\cdot s] \tag{1}$$

In Equation 1, $\dot{\gamma}$ denotes the local shear rate (in s^{-1}), while μ_0 and μ_∞ represent the viscosity values at zero and infinitely large shear rates, respectively. The relaxation time (λ) and the power index (n) are the further model parameters. For human blood, the model parameters are provided as: $\mu_0 = 0.056$ Pa·s, $\mu_\infty = 0.00345$ Pa·s, $\lambda = 3.313$ s, and $n = 0.3568$.[29] The blood density (ρ) was assumed to be 1060 kg/m^3.

To be meaningful, an LES study requires a sufficiently fine grid resolution compared to the turbulent length scales. The smallest length scale of turbulence is the so-called Kolmogorov length scale (η). For a Newtonian fluid η is defined by the following expression[23]

$$\eta = \left(\frac{\nu^3}{\varepsilon}\right)^{1/4} \tag{2}$$

where ν and ε denote the molecular kinematic viscosity and the dissipation rate of turbulence kinetic energy, respectively. An LES analysis does not contain explicit information on ε. For obtaining an estimation on the Kolmogorov length scales, RANS calculations were performed in

advance, using the four-equation transitional SST turbulence model,[30,31] which can cope with the transitional flow behavior (flow being laminar or turbulent in different regions), and where the ε field is explicitly obtained by solving a modelled transport equation. Here a Newtonian material behavior was assumed, since the model does not accommodate for a non-Newtonian behavior. However, in doing so, the lowest possible viscosity (μ_∞) was assigned as the fluid viscosity for assuring that the most demanding conditions are covered. The characteristic local mesh size (Δ) of the computational grid was obtained by the cube root of the local cell volume (V) of the three-dimensional finite volume mesh, that is,

$$\Delta = (V)^{1/3} \tag{3}$$

The grid resolution was quantified by the so-called "grid index" (GI), which is the ratio of the Δ to the η, that is,

$$GI = \frac{\Delta}{\eta} \tag{4}$$

According to the investigation of Celik et al,[32] for an accurate LES prediction, the following criterion needs to be fulfilled by the computational grid

$$GI \leq 25 \tag{5}$$

Thus, within the above-mentioned RANS framework using the transitional SST turbulence model, the finite volume mesh was locally refined in such a way that the condition (5) was fulfilled everywhere in the solution domain. In the present analysis, the criterion was applied even more stringently, requiring the fulfillment of $GI \leq 5$, so that the grid was no doubt adequately fine for an LES investigation. The resulting grids were then used in the subsequent unsteady LES analysis considering the non-Newtonian blood behavior. The grids generated this way that turned out to have nearly 10 million finite volume cells.

Not only the spatial but also the temporal resolution should be sufficiently fine. A time-step size (Δt) of 10^{-5} s was applied, which resulted in cell Courant numbers[25,26] substantially lower than unity, which can be considered to be adequate for the present analysis. In time discretization a second-order accurate backward differencing scheme[25,26] was used. For the spatial discretization of the convective terms, the third-order accurate Monotonic Upwind Scheme for Conservation Laws (MUSCL) scheme[25,26] was applied. The velocity-pressure coupling was treated by the Semi-Implicit Method for Pressure-Linked Equations-Consistent (SIMPLEC) pressure-correction algorithm.[25,26]

The potential of hemolysis associated with the design of each device was computationally assessed by the dimensionless modified index of hemolysis (MIH).[34] The MIH measures the increase in plasma-free hemoglobin, normalized by the total quantity of hemoglobin in the volume of blood in the circuit. By definition, $MIH = 1$ means that one millionth of the erythrocytes in the circuit are damaged.[34] For the calculation of MIH, the method proposed by Garon and Farinas[35] was used, where MIH was estimated from

$$MIH = D \cdot 10^6 \tag{6}$$

In the above equation, D is related to a linearized damage fraction. Garon and Farinas[35] propose the following relationship for the calculation of D

$$D = \left[\frac{1}{Q} \int_V \sigma \, dV \right]^{0.785} \tag{7}$$

In Equation 7, V denotes the device volume and Q is the volume flow rate through the device. The quantity σ to be integrated over the device volume (Equation 7), represents the stress responsible for blood damage. This is related to the scalar stress τ based on the Von Mises criterion through the following relationship[35]

$$\sigma = \left(3.62 \times 10^{-7} \cdot \tau^{2.416}\right)^{\frac{1}{0.785}} \tag{8}$$

with

$$\tau = \sqrt{\frac{(\sigma_1 - \sigma_2)^2 + (\sigma_2 - \sigma_3)^2 + (\sigma_3 - \sigma_1)^2}{2}} \tag{9}$$

where σ_1, σ_2, and σ_3 denote the principal stresses.

3 | TEST CASES CONSIDERED

The hardshell reservoirs corresponding to Sorin Dual Avant and LivaNova Inspire are denoted as reservoir 1 (R 1) and reservoir (R 2), respectively. The solution domains for the modelled geometries of the hardshell reservoirs are shown in Figure 1, in perspective view, where the red colored surface represents the inlet boundary of the domain.

The modelled geometries (Figure 1) closely resemble the geometries of the two existing products. However, it shall also be noted that the resemblance is not perfect and contains some simplifications in detail. For both cases a filling level of 1000 mL was assumed. The solution domain contains the fluid region only. Therefore, the geometries shown in Figure 1 cover the geometry lower than the level of 1000 mL filling.

Outlines of the solution domains are shown in Figure 2 in side view, where the different boundary types are also

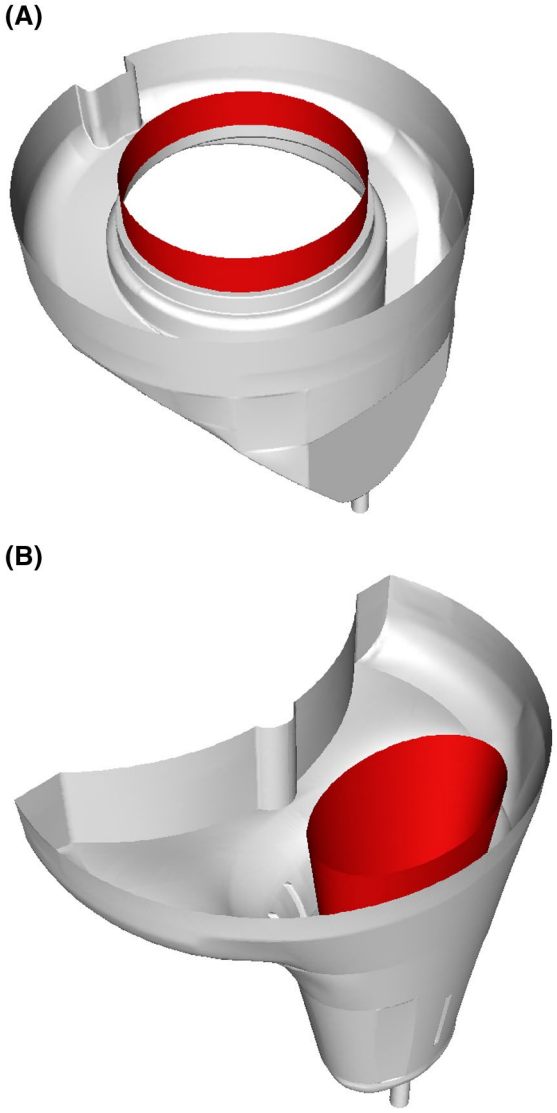

FIGURE 1 Three-dimensional views of solution domains for modelled hardshell venous reservoir geometries in perspective view, A, Reservoir 1, B, Reservoir 2. Red: inlet boundaries. [Color figure can be viewed at wileyonlinelibrary.com]

indicated (the inlet boundaries were already indicated as the red colored surfaces in Figure 1). In Figure 2, the different concepts for the blood inflow between the two hardshell reservoir designs are also indicated by the red arrows. In R 1, blood is introduced vertically upward at the base of the device (Figure 2A). In R 2, the blood is introduced by a long lance (indicated by a dashed line) in the vertically downward direction behind the membrane (Figure 2B). For both cases, a volume flow rate of 4 L/s was assumed. As the velocity distribution over the inlet boundary was not known in detail, a homogeneous velocity distribution normal to the inlet surface was assumed. In general, flow resistance leads to flow homogenization. Thus, due to the comparably high flow resistances by the membranes, a homogeneous velocity distribution may be assumed to be reasonable.

The outlet boundary was placed at a section of the drainage tube, at a position nearly 3-5 diameters downstream from the tube inlet section (Figure 2). At the outlet, a constant gauge pressure was applied along with zero normal gradient for the remaining variables. The free-surface was modelled as a plain, "slip" boundary. Thus, any interaction between blood and air across this surface was neglected, such as wave formation, or shear stresses. On the walls, no-slip conditions apply.

At this stage, a difference in the geometries shall be emphasized, which turns out to be important for the flow characteristics. This is the way how the drainage tube is connected with the reservoir. For R 1, the strongly inclined reservoir bottom makes a large angle with the tube axis, resulting in a sharp corner at their connection (Figure 2A). For R 2, the horizontal reservoir bottom makes a right angle with the tube axis without resulting in such a sharp angle at the connection (Figure 2B).

4 | RESULTS AND DISCUSSION

4.1 | Preliminary RANS results using the transitional SST turbulence model

As already explained above, this part of the analysis was performed for obtaining an initial impression of turbulence generation as well as for designing a computational grid that can sufficiently resolve the turbulent scales. Since state-of-the-art turbulence models, like the presently applied four-equation transitional SST model, cannot accommodate for non-Newtonian behavior, a Newtonian blood behavior was assumed. Here, the constant blood viscosity was assumed to be given by μ_∞. The Reynolds number (Re) can be calculated at the inlet and the outlet boundaries from $\mathrm{Re} = \rho UL/\mu_\infty$, where U is the local cross-sectional bulk velocity and L is the corresponding representative length scale. At the inlet, defining L to be the height of the inflow boundary, a Reynolds number lower than or about 100 can be calculated, which implies, locally, a laminar flow. At the drainage tube, defining L to be the tube diameter, due to the much higher local flow velocity, the local Reynolds number turns out to be about 3300. This is above 2300, which is generally assumed to be the upper limit of the laminar mode of the pipe flow for Newtonian flow. Based on this, turbulent flow at the exits of the reservoirs can be expected. As the flow continuously accelerates from the inlet toward the outlet boundary, it is possible that transitional flow and onset of turbulence can occur within the device, depending on the geometry. The present RANS analysis based on a four-equation transitional SST turbulence model is the preliminary step for this investigation. Assuming isotropic turbulence, the representative turbulent fluctuation velocity in magnitude (u') can be obtained from

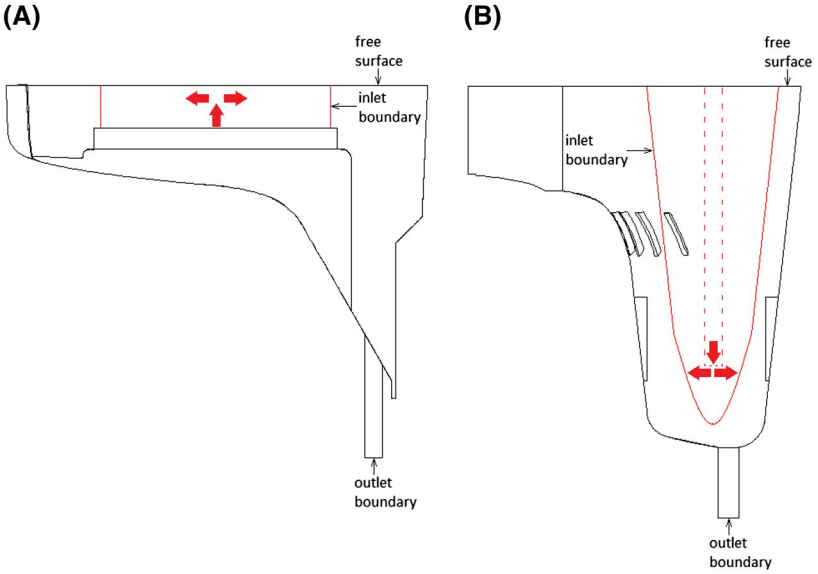

FIGURE 2 Outlines of solution domains for modelled hardshell venous reservoir geometries in side view, A, Reservoir 1, B, Reservoir 2. Continuous red lines indicate the inlet boundaries in the respective geometry. Dashed red line in (B) indicates the blood introducing lance. Red arrows indicate the change of main blood flow direction from vertical to horizontal within the apparatus. This is added as background information for better understanding but not relevant for the present calculations, since the present solution domains start at the indicated inlet boundaries (red lines). [Color figure can be viewed at wileyonlinelibrary.com]

FIGURE 3 Distribution of turbulence intensity, Tu (%), in the midline plane of the device, A, Reservoir 1, B, Reservoir 2. [Color figure can be viewed at wileyonlinelibrary.com]

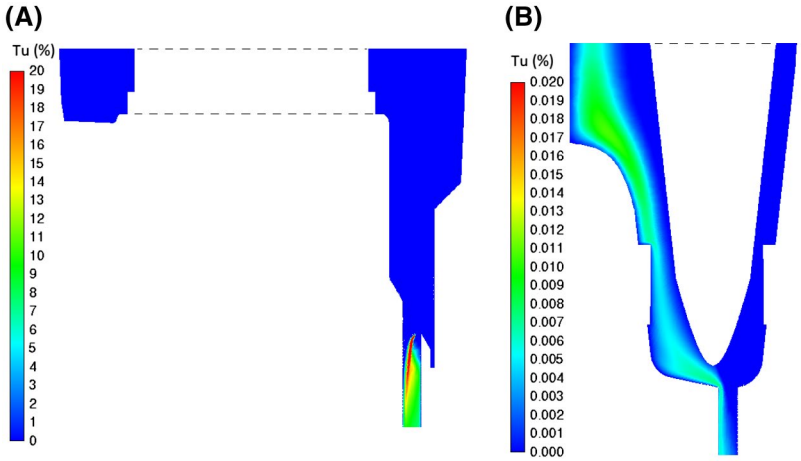

the calculated (transitional SST model) turbulence kinetic energy (k) as

$$u' = \sqrt{\frac{2}{3}k} \tag{10}$$

Based on a reference time-averaged flow velocity U_{ref}, a turbulence intensity (Tu) can be defined as

$$\text{Tu} = \frac{u'}{U_{\text{ref}}} \tag{11}$$

As the reference time-averaged flow velocity, the bulk flow speed at the drainage tube was used (U_{ref} = 1.33 m/s). The distribution of the percentage turbulence intensity (Tu) in a plane through the middle of the device is displayed in Figure 3. Please note that the scales of the plots for the two devices differ by a factor of 1000. Figure 3B shows that practically no turbulence is generated in R 2. For R 1, it can be observed that there is no substantial turbulence generation within the reservoir. However, just at the exit, a considerable amount of turbulence is generated (the maximum value is 33%), due to the strong shear layer caused by the sharp corner and induced inhomogeneous flow field (Figure 3A).

4.2 | LES results

As already mentioned above, these calculations were performed considering the non-Newtonian blood behavior

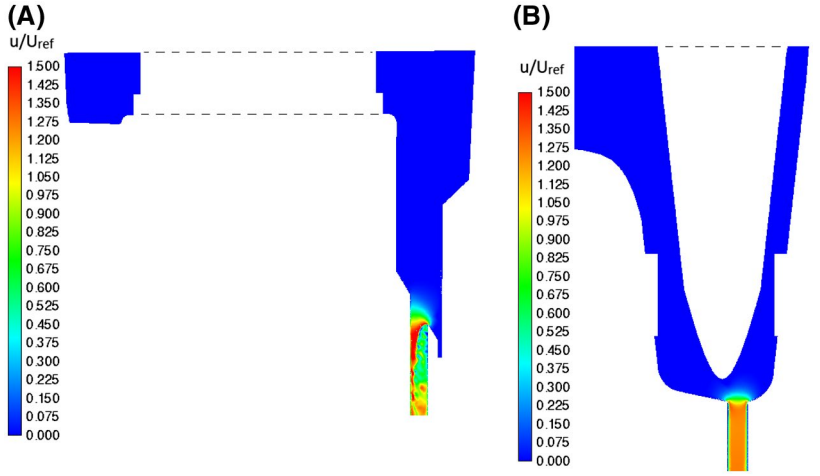

FIGURE 4 Distribution of nondimensional instantaneous velocity magnitude in the midline plane of the device, A, R 1, B, R 2. [Color figure can be viewed at wileyonlinelibrary.com]

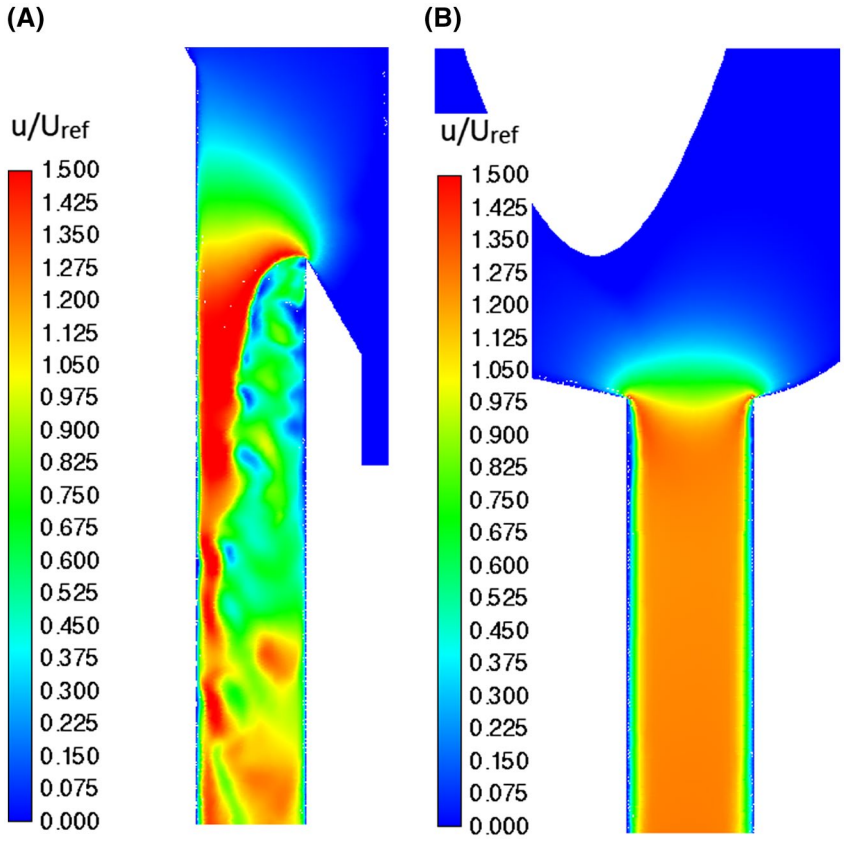

FIGURE 5 Distribution of nondimensional instantaneous velocity magnitude in the midline plane of the device as detail plot near the exit region, A, R 1, B, R 2. [Color figure can be viewed at wileyonlinelibrary.com]

(Equation 1). Distributions of the instantaneous velocity magnitude in planes through the midline plane of the devices, as predicted by LES, are presented in Figure 4, in nondimensional form (nondimensionalized by U_{ref}). It can be observed that the velocities in most parts of both reservoirs are quite low. A noticeable flow acceleration is observed only in a small region just upstream of the entrance of the tube. The instantaneous distribution of the velocity field is quite inhomogeneous for R 1 in the tube, indicating a high turbulence level generated by the unfavorable entrance conditions of the flow from the reservoir into the tube (Figure 4A). This is in accordance with observations based on the preceding RANS calculation using the transitional SST model (Figure 3A). On the contrary, the instantaneous velocity distribution for R 2 is very homogeneous, which indicates negligibly low turbulence levels (Figure 4B).

For clarity, the velocity plots shown in Figure 4 are recapitulated as detail plots for the exit region in Figure 5. The highly turbulent flow structure for R 1 (Figure 5A) and the quite smooth flow of R 2 in comparison (Figure 5B), can be observed again.

TABLE 1 Nondimensional pressure drops through the evaluated devices predicted by LES and RANS

	$2\Delta p/(\rho U_{ref}^2)$	
	LES	**RANS (transitional SST)**
R 1	2.34	2.30
R 2	1.65	1.65

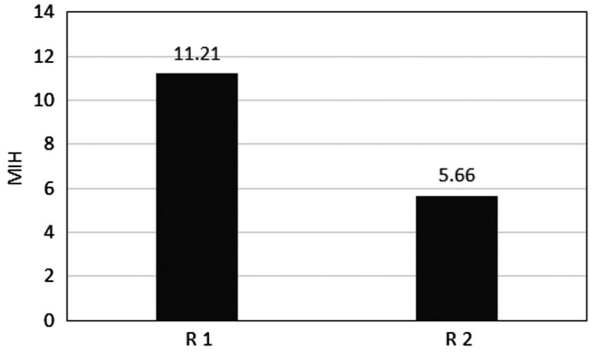

FIGURE 6 Predicted MIH values for the design of the two evaluated devices

The time-averaged pressure drops (Δp) in nondimensional form (nondimensionalized by $\rho U_{ref}^2/2$) as calculated by LES and RANS (transitional SST model) between the inlet and outlet boundaries of the devices are presented in Table 1. The results demonstrate that the pressure drop of R 1 is considerably larger (approx. 40%) compared to R 2. Moreover, LES and RANS predictions agree quite well. There is a perfect agreement of the LES results with RANS results for R 2, whereas some difference is observed for R 1. These findings can be seen as further evidence of the unsteady nature of the flow of R 1 compared to the predominantly steady flow of R 2.

The predicted time-averaged MIH values for the two devices are presented in Figure 6. A considerable difference between the two designs can be observed.

The calculated hemolysis potential of R 1 ranges around values nearly double those of R 2, according to the MIH criterion (Figure 6). However, compared to other components of the CPB circuit where much higher MIH values are observed, for example, cannulas (MIH ~ 100) or blood pumps (MIH ~ 1000),[35] the present values are rather low and do not necessarily indicate a severe problem in this respect. As already stated above, blood damage during the flow through the membranes and further possible causes of hemolysis were not considered here. The present prediction (Figure 6) refers purely to the mechanical causes of the reservoir design. The comparatively inferior performance of R 1 is due to the design of the entrance section to the drainage tube and can be improved by a corresponding geometry modification.

5 | CONCLUSIONS

Blood flow characteristics of two commercially available hardshell venous reservoirs, Sorin (today: LivaNova) Dual Avant (R 1), and LivaNova Inspire (R 2), were computationally investigated.

The change in design from R 1 to R 2 improved the predicted turbulence generation strongly. For R 1, a considerable turbulence generation was predicted, which was caused by the sharp edge at the connection to the drainage tube, resulting in a sharp shear layer and a 40% larger pressure drop. When a quantification of the hemolysis potential was evaluated, R 1 led to MIH values approximately twice those observed in R 2 (11.21 vs. 5.66), due to the aforementioned unfavorable flow pattern. Although the predicted MIH values are still quite low when compared to other components of the CPB circuit such as cannulas and pumps, the MIH of R 1 may be improved by a corresponding geometry modification.

The change of the design from R 1 to R 2 improved the hemocompatibility substantially, demonstrating the critical impact of hardshell venous reservoir design on their function in terms of hemodynamic behavior. Following these CFD based insights, an in vivo study—ideally involving standardized conditions of a large animal study—are needed to further elaborate the clinical relevance of the herein presented findings.

ACKNOWLEDGMENTS

The financial support by CORMED Medizintechik (Rüthen, Germany) (to P.A.) is gratefully acknowledged. Dr. Khawar J. Syed is gratefully acknowledged for his help in English editing.

CONFLICT OF INTEREST

The authors declare that they have no conflicts of interest with the contents of this article.

AUTHOR CONTRIBUTIONS

Data generation, data analysis and interpretation, drafting of the manuscript: A.C.B.
Conceptual design, data generation: T.F.
Critical revision of the manuscript: A.A.
Review of the manuscript and clinical input: A.L.
Concept/design, critical revision of the manuscript, securing funding: P.A.

ORCID

Ali Cemal Benim https://orcid.org/0000-0002-8642-2225
Payam Akhyari https://orcid.org/0000-0002-6452-8678

REFERENCES

1. Paparella D, Galeone A, Venneri MT, Coviello M, Visicchio G, Cappabianca G, et al. Blood damage related to cardiopulmonary bypass: in vivo and in vitro comparison of two different centrifugal pumps. ASAIO J. 2004;50:473–8.

2. Blustein D, Chandran KB, Manning KB. Towards non-thrombogenic performance of blood recirculating devices. Ann Biomed Eng. 2010;38:1236–56.
3. Venema LH, Sharma AJ, Simons AP, Bekers O, Weerwind PW. Contemporary oxygenator design relative to hemolysis. J Extra Corpor Technol. 2014;46:212–6.
4. Jegger D, Horisberger J, Jachertz M, Seigneul I, Tozzi P, Delay D, et al. A novel device or reducing hemolysis provoked by cardiotomy suction during open heart cardiopulmonary bypass surgery: a randomized prospective study. Artif Organs. 2007;31:23–30.
5. Benim AC, Nahavandi A, Assmann A, Schubert D, Feindt P, Suh SH. Simulation of blood flow in human aorta with emphasis on outlet boundary conditions. Appl Math Model. 2011;35:3175–88.
6. Benim AC, Gül F, Assmann A, Akhyari P, Lichtenberg A, Joos F. Validation of loss-coefficient-based outlet boundary conditions for simulating aortic flow. J Mech Med Biol. 2016;16; 15 pages. https://doi.org/10.1142/S0219519416500111.
7. Assmann A, Benim AC, Gül F, Lux P, Akhyari P, Boeken U, et al. Pulsatile extracorporeal circulation during on-pump cardiac surgery enhances aortic wall shear stress. J Biomech. 2012;45: 156–63. https://doi.org/10.1016/j.jbiomech.2011.09.021.
8. Assmann A, Gül F, Benim AC, Joos F, Akhyari P, Lichtenberg A. Dispersive aortic cannulas reduce aortic wall shear stress affecting atherosclerotic plaque embolization. Artif Organs. 2015; 39:203–11.
9. Janela J, Moura A, Sequieira A. A 3D non-Newtonian fluid-structure interaction model for blood flow in arteries. J Comput Appl Math. 2010;234:2783–91.
10. Rispoli VC, Nielsen JF, Nayak KS, Carvalho JLA. Computational fluid dynamics simulations of blood flow regularized by 3D phase contrast MRI. BioMed Eng OnLine. 2015;14; 23 pages. https://doi.org/10.1186/s12938-015-0104-7.
11. Zhong L, Zhang JM, Su B, Tan RS, Allen JC, Kassab GS. Application of patient-specific computational fluid dynamics in coronary and intra-cardiac flow simulations: challenges and opportunities. Front Physiol. 2018;9; 17 pages. Article 742 https://doi.org/10.3389/fphys.2018.00742.
12. Apel A, Paul R, Klaus S, Siess T, Reul H. Assessment of hemolysis related quantities in a microaxial blood pump by computational fluid dynamics. Artif Organs. 2001;25:341–7.
13. Yano T, Sekine K, Mitoh A, Mitamura Y, Okamoto E, Kim DW, et al. An estimation method of hemolysis within an axial blood pump by computational fluid dynamics analysis. Artif Organs. 2003;27:920–5.
14. Song X, Throckmorton AL, Wood HG, Antaki JF, Olsen DB. Computational fluid dynamics prediction of blood damage in a centrifugal pump. Artif Organs. 2003;27:938–41.
15. Zhang J, Gellmann B, Koert A, Dasse KA, Gilbert RJ, Griffith BP, et al. Computational and experimental evaluation of the fluid dynamics and hemocompatibility of the CentriMag blood pump. Artif Organs. 2006;30:168–77.
16. Chandran KB. Role of computational simulations in heart valve dynamics and design of valvular prostheses. Cardiovasc Eng Technol. 2010;1:18–38.
17. Kadhim SK, Nasif MS, Al-Kayiem HH, Al-Waked R. Computational fluid dynamics simulation of blood flow profile and shear stresses in bileaflet mechanical heart valve by using monolithic approach. Simulation. 2018;94:93–104.
18. Khalili F, Gamage PPT, Sandlerm RH, Mansy HA. Adverse hemodynamic conditions associated with mechanical heart valve leaflet immobility. Bioengineering. 2018;5:74. https://doi.org/10.3390/bioengineering5030074.
19. Spühler JH, Jansson J, Janson N, Hoffman J. 3D fluid-structure interaction simulation of aortic valves using a Unified Continuum ALE FEM model. Front Physiol. 2018;9; 16 pages. Article 363. https://doi.org/10.3389/fphys.2018.00363.
20. Gage KL, Gartner MJ, Burgreen GW, Wagner WR. Predicting membrane oxygenator pressure drop using computational fluid dynamics. Artif Organs. 2002;26:600–7.
21. Jones CC, McDonough JM, Capasso P, Wang D, Rosenstein KS, Zwischenberger JB. Improved computational fluid dynamic simulations of blood flow in membrane oxygenators from X-ray imaging. Ann Biomed Eng. 2013;41:2088–98.
22. Pelosi A, Sheriff J, Stevanella M, Fiore GB, Bluestein D, Redaelli A. Computational evaluation of the thrombogenic potential of a hollow-fiber oxygenator with integrated heat exchanger during extracorporeal circulation. Biomech Model Mechanobiol. 2014;13:349–61.
23. Durbin PA, Reif BAP. Statistical theory and modelling for turbulent flows. 2nd ed. Chichester, UK: Wiley; 2011.
24. Wilcox DC. Formulation of the k–ω turbulence model revisited. AIAA J. 2008;46:2823–38.
25. Versteeg HK, Malalasekera W. An introduction to computational fluid dynamics—the finite volume method. 2nd ed. Harlow, UK: Pearson; 2007.
26. ANSYS Fluent Theory Guide. Release 18.0. Canonsburg, PA: ANSYS Inc; 2017. Available from: www.ansys.com
27. Sagaut P. Large Eddy simulation for incompressible flows—an introduction. 2nd ed. Berlin, Germany: Springer; 2002.
28. Grinstein FF, Margolin LG, Rider WJ. Implicit large Eddy simulation. Cambridge University Press; 2007.
29. Tabakova S, Kutev N, Radev S. Application of Carreau viscosity model to oscillatory flow in blood vessels. AIP Conf Proc. 2015;1690:040019. https://doi.org/10.1063/1.4936726.
30. Menter FR, Langtry R, Volker S. Transition modelling for general purpose CFD codes. Flow Turbul Combust. 2006;77:277–303.
31. Oclon P, Lopata S, Nowak M, Benim AC. Numerical study on the effect of inner tube fouling on the thermal performance of high-temperature fin-and-tube heat exchanger. Prog Comput Fluid Dyn Int J. 2015;15:290–306.
32. Celik IB, Cehreli ZN, Yavuz I. Index of resolution quality for large eddy simulations. J Fluids Eng. 2005;127:949–58.
33. Van Leer B. Towards the ultimate conservative difference scheme. V. A second order sequel to Godunov's method. J Comput Phys. 1979;32:101–36.
34. Mueller MR, Schima H, Engelhardt H, Salat A, Olsen DB, Losert U, et al. In vitro hematological testing of rotary blood pumps: remarks on standardization and data interpretation. Artif Organs. 1993;17:103–10.
35. Garon A, Farinas MI. Fast three-dimensional numerical hemolysis approximation. Artif Organs. 2004;28:1016–25.

How to cite this article: Benim AC, Frank T, Assmann A, Lichtenberg A, Akhyari P. Computational investigation of hemodynamics in hardshell venous reservoirs: A comparative study. *Artif Organs*. 2020;44:411–418. https://doi.org/10.1111/aor.13593